Thin Solid Films 660 (2018) 365–372

Contents lists available at ScienceDirect

Thin Solid Films

journal homepage: www.elsevier.com/locate/tsf

Terrace site hydroxylation upon water dimer formation on monolayer NiO/Ag(100)

Chris Arble[a], Xiao Tong[b], Livia Giordano[c], John T. Newberg[a,*], Anna Maria Ferrari[d,*]

[a] Department of Chemistry and Biochemistry, University of Delaware, Newark, Delaware 19716, USA
[b] Brookhaven National Laboratory, Center for Functional Nanomaterials, Upton, New York 11973, USA
[c] Dipartimento di Scienza dei Materiali, Università di Milano-Bicocca, Milano 20125, Italy
[d] Dipartimento di Chimica IFM, NIS-Nanostructured Interfaces and Surfaces-Centre, Università di Torino, Torino 10125, Italy

ARTICLE INFO

Keywords:
X-ray photoelectron spectroscopy
Density functional theory
Nickel oxide
Monolayer
Water dissociation

ABSTRACT

The interaction of water vapor with monolayer NiO/Ag(100) was examined using both experimental and computational techniques. Initial film growth was characterized by scanning tunneling microscopy and low energy electron diffraction showing the formation of NiO(1 × 1). X-ray photoelectron spectroscopy (XPS) reveals that the initial film was mainly composed of NiO oxide with a small amount of hydroxyl groups (OH) attributed to the dissociation of background water vapor at highly reactive edge sites. Density functional theory (DFT) reveals that the adsorption of a water monomer on NiO/Ag(100) terrace sites prefers to be in the molecular rather than the dissociate state. XPS results indicate that upon exposing the oxide film to high water vapor pressures (maximum 333.3 Pa), extensive hydroxylation occurs which is attributed to water dissociation at terrace sites. DFT reveals that upon aggregation of water monomers to dimers at the oxide interface the dissociated dimer is energetically stable. The results herein are consistent with previous MgO/Ag(100) studies, further revealing that for certain metal oxides the formation of water dimers at the metal oxide-vapor interface is a key mechanism leading to extensive terrace site hydroxylation.

1. Introduction

Nickel oxide (NiO) films have been used in a variety of technological applications ranging from optoelectronic devices [1], fuel cells [2], magnetic pinning layers [3] and sensors [4]. The dissociation of water at metal oxide interfaces leads to hydroxyl groups, thereby significantly altering chemistry and properties of the metal oxide interface [5]. Supported metal oxide thin films can react differently towards water depending on the film thickness [6]. This suggests that the efficacy for water dissociation to occur can be fundamentally controlled. It is therefore important to understand the extent to which metal oxides hydroxylate on a molecular level upon exposure to water. Herein we examine the interaction of water with monolayer NiO supported by Ag (100) in order to reveal the mechanism of water adsorption and dissociation.

A number of vacuum-based surface science studies have examined the interaction of water with an NiO(100) single crystal and Ag(100) supported NiO films utilizing X-ray photoelectron spectroscopy (XPS), ultraviolet photoelectron spectroscopy, temperature program desorption and low-energy electron diffraction (LEED) [7–13]. These experiments suggest that defect sites are reactive towards the dissociation of water, while stoichiometric terrace sites of the NiO(100) interface are unreactive upon exposure to water vapor. The lack of extensive reactivity could be due to the low water vapor pressures used to expose samples under high vacuum.

A number of molecular simulation methods have been utilized to examine the interaction of water with NiO(100), including semi-empirical self-consistent field molecular orbital method [14, 15] and Gradient-corrected approximation with Hubbard correction [16, 17]. Simulation results agree with the aforementioned surface science studies, indicating that water adsorption at NiO(100) terrace sites are predicted to be more favorable in the molecular state rather than the dissociated state for low water coverages. However, there is evidence that multilayer water adsorption, a representation of NiO(100) in contact with bulk water, leads to partial dissociation within the first water layer at 293 K [18]. The aforementioned molecular simulations were performed on bulk terminated NiO(100) [14–18], while there are currently no molecular simulations that have examined the interaction of water with stoichiometric terrace sites of an Ag(100) supported NiO film.

Given the lack of NiO(100) terrace site reactivity observed experimentally for low water vapor pressures exposures [7–13], we

* Corresponding authors.
E-mail addresses: jnewberg@udel.edu (J.T. Newberg), anna.ferrari@unito.it (A.M. Ferrari).

https://doi.org/10.1016/j.tsf.2018.06.033
Received 16 March 2018; Received in revised form 13 June 2018; Accepted 15 June 2018
Available online 18 June 2018
0040-6090/

hypothesize that exposure to higher water vapor pressures may lead to additional reactivity at terraces. Herein we use a combination of experimental and computational techniques to examine the interaction of water with submonolayer NiO(1 × 1) deposited onto Ag(100). Scanning tunneling microscopy (STM) and LEED were utilized to determine film quality while the chemical composition and extent of metal oxide hydroxylation was monitored using XPS following *in-vacuo* exposures to water vapor. The efficacy for water to dissociate at (100) terrace sites on an Ag(100) supported NiO monolayer was examined using hybrid functional density functional theory (DFT).

2. Methods

2.1. Experiments

Experiments were performed at Brookhaven National Laboratory Center for Functional Nanomaterials using an ultra-high vacuum (UHV) system consisting of a STM chamber, preparation chamber, and a fast entry load lock chamber. LEED images (Specs, ErLEED 150) were captured at room temperature in the preparation chamber. STM experiments (RHK, VT-STM/AFM) were performed at room temperature with images captured under pressures of $< 4 \times 10^{-8}$ Pa. STM tips were composed of tungsten that were electrochemically etched in a 0.10 M KOH solution and then sputtered *in-vacuo*. STM images were acquired under constant current mode with home-built electronics and GXSM software. STM images were processed using ImageJ software [19]. Due to the lack of atomic resolution for this STM setup, initial investigations did not prove valuable to assess changes in the NiO film morphology before and after water exposures. Thus, the focus of STM measurements herein were on characterizing the morphology of the initial NiO film deposition.

XPS spectra were collected in the preparation chamber with base pressures $< 2.6 \times 10^{-7}$ Pa using Al K_α X-rays from a twin anode source (SPECS, XR50) and hemispherical electron energy analyzer (SPECS, PHOIBOS 100). Photoelectrons were collected at 0° relative to the sample surface normal. Ag 3d, O 1s, Ni 2p and C 1 s spectra were collected using 20 eV pass energy. All spectra were calibrated to Ag 3d(5/2) at 368.3 eV [20]. XPS peaks were analyzed using peak fitting software (CasaXPS, v2.3.17) with a Shirley background and Gaussian (80%) Lorentzian (20%) peak fits.

The substrate was secured through a Molybdenum ring that mounted onto the outer lip of a hat shaped Ag(100) single crystal (Mateck, 99.999%, < 0.4° polishing). The Ag substrate was cleaned with cycles of sputtering in 1.3×10^{-3} Pa Ar^+ at 1.5 kV and subsequently annealed to 700 K. NiO has a 2% lattice mismatch with Ag(100) [21] and forms high quality (1 × 1) films on Ag(100) depending on the O_2(g) pressure (or dosage) and substrate temperature [22–29]. Herein NiO thin films were deposited by electron-beam evaporation (Mantis Deposition LTD, QUAD-EV-C Mini) from an Ni rod (ESPI, 99.995%) in 1.3×10^{-4} Pa O_2 at a rate of ~1·ML·min^{-1} monitored using a quartz crystal microbalance (Inficon, Qpod). The sample substrate was held at room temperature (300*K*) during deposition, followed by annealing in 1.3×10^{-3} Pa O_2 to 600 K for 10 min. Post annealing NiO above 550 K has been shown to induce a morphology change from (2 × 1) to (1 × 1) on Ag(100) [28].

Water vapor exposures were performed at 300 K6 in the fast entry chamber which was baked and maintained a base pressure of $< 2.6 \times 10^{-6}$ Pa. The fast entry chamber was equipped with a precision leak valve, behind which was a custom glass bulb containing 18.2 MΩ-cm water (Aqua Solutions, 2122A) which was freeze-degassed at least three times prior to the start of experiments. After exposure to water vapor, the load lock chamber was pumped down and the sample was transferred for XPS analysis under UHV.

2.2. Simulations

DFT calculations were performed with a periodic approach, using a localized Gaussian type functions (GTF) basis set implemented in the CRYSTAL14 code [30]. For surface calculations, CRYSTAL adopts periodic slab models characterized by two infinite dimensions (x and y) and a finite thickness. An Ag slab, at the experimental lattice parameter, has been used to model the metal substrate. We have verified that the use of the optimized lattice parameters for Ag does not change the results. The NiO overlayer is adsorbed on both sides of a Ag 5-layer slab. This model has been shown to provide a satisfactory description of the metal substrate in many cases of metal-oxide interactions [31–36]. The properties of NiO monolayer on Ag(100) were modeled with a (2 × 1) unit cells for the most stable antiferromagnetic magnetic configurations with opposite spin on the two Ni^{2+} ions.

Adsorption of an isolated water molecule was modeled using a (2√2 × 2√2)R45° supercell (8 Ni and 8 O) with respect to the Ag(100) surface and corresponds to a coverage Θ = 1/8 ML (the same coverage has been considered for adsorption at the NiO (100) surface). All coordinates of the adsorbates, oxide films and the Ag substrate were allowed to relax while keeping fixed the lattice parameters. Two different GTF basis sets have been employed: basis set A of triple zeta quality used for geometry relaxations and a larger one, B, of quadruple zeta quality for the valence, has been employed for accurate estimates of energetics. Basis A consisted of all-electron [311-1]/(3s1p) and [511111-411-1]/(6s3p1d) functions for H and O [37], respectively, Hay-Wadt relativistic small core pseudopotentials [38] (15 electrons) together with [31111-311]/(5sp3d) contracted GTF functions for Ni and Hay-Wadt relativistic small core pseudopotentials [38] (19 electrons) together with [2111-31]/(4sp2d) contracted GTF functions for Ag. Basis B consisted of all electron [6211111-4111-11-1]/(7s4p2d1f), [3111-11-1]/(4s2p1d) for O and H [39], [84111111-621,111-3111-1]/(10s6p4d1f) GTFs for Ni [40] while Ag basis set was unchanged. With basis A the basis set superposition error (BSSE) has been checked to be < 0.15 eV but with basis B it did not exceed 0.05 eV.

In CRYSTAL calculations, one of the crucial points of the treatment is the truncation of the infinite Coulomb and exchange series. These truncations are controlled by five parameters (see ref. 30 for an explicit description of the way they act), indicated as Ti, whose safe values are set to 10^{-7} (T1-T3), 10^{-8} (T4) and 10^{-16} (T5). The convergence threshold for SCF energy was set to 10^{-8} Ha. The reciprocal space was sampled according to a regular sub-lattice determined by the shrinking factor [30] which was set to 12 (50 independent k-points in the irreducible part of the Brillouin zone) for the (2√2 × 2√2)R45° supercell. A Fermi-Dirac smearing procedure has been adopted with the smearing parameter of 0.01 Hartree (0.27 eV). Geometry optimizations were carried out using analytical gradients with respect to atomic coordinates and convergence threshold for atomic forces was set to 0.005 eV/Å. BSSE was estimated by applying the standard counterpoise method [41]. The hybrid PBE0 [42] functional has been used for all calculations since it has been reported to provide a feasible description of the adsorption properties of surface adsorbates [43–45]. Dispersive corrections have not considered since the interactions studied in this work are not purely dispersive but largely dominated by electrostatics effects. Previous works have proved that this kind of interactions is well described by PBE0 providing excellent comparison with experimental data [43–45]. In addition test calculations have also been performed with B3PW functional [46, 47], found to be particularly suitable for the study of magnetic metal/oxide heterostructures [31].

3. Results and discussion

An STM image of a freshly prepared NiO/Ag(100) film collected at a positive bias of +2.5 V is shown in Fig. 1a with an estimated coverage of 0.5 ML. The surface is composed of square and rectangular islands (dark) on the Ag(100) substrate (bright background) which extend

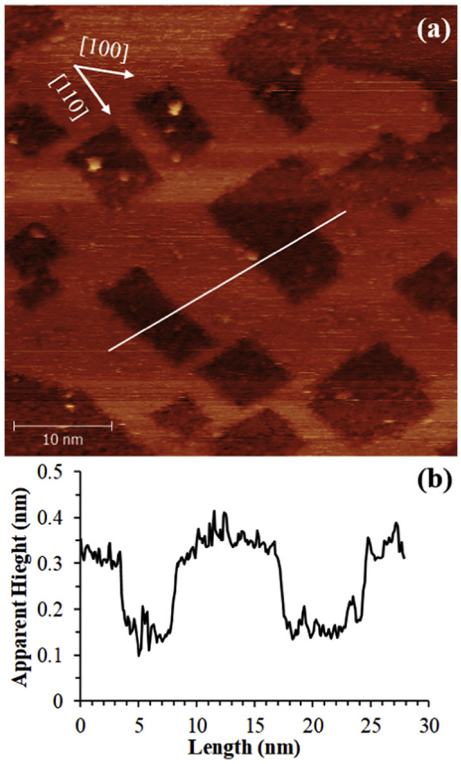

Fig. 1. (a) STM image of NiO film collected at +2.5 V and 0.5 nA. The principal crystallographic directions are indicated. (b) Topological plot of white line in (a).

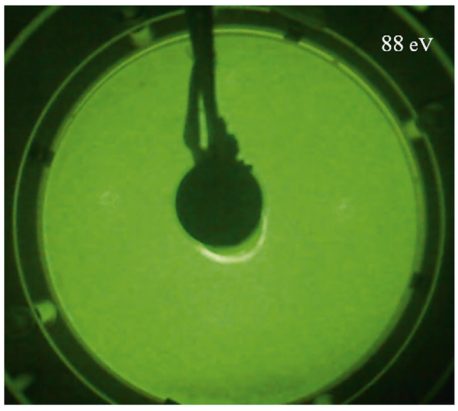

Fig. 2. LEED image of an annealed NiO(100) film.

laterally ranging in size from about 5 to 20 nm. The imaging of dark NiO islands on Ag(100) is consistent with previous STM studies at low positive bias [24, 48]. A plot of tunneling current versus bias shows that the electronic states of the NiO are accessed at ~3 V and above [24]. Thus, the dark images for the islands stem from a lowering of the tunneling current relative to the metallic Ag(100) substrate. This decrease in tunneling current gives rise to a dip in line traces across the NiO islands (Fig. 1b) which give an apparent height of ~0.2 nm. In addition to isolated islands, there are regions of extended NiO films across the surface that are several 10's of nm across (see upper right corner of Fig. 1a). The cubic nature of the NiO islands is indicative of a (1 × 1) structure on Ag(100), confirming that our post annealing procedure produces NiO(1 × 1) structures [28]. This is further evidenced by performing LEED on a freshly prepared film which displayed (1 × 1) diffraction pattern (Fig. 2).

During NiO film deposition the O_2(g) pressure was chosen to be held

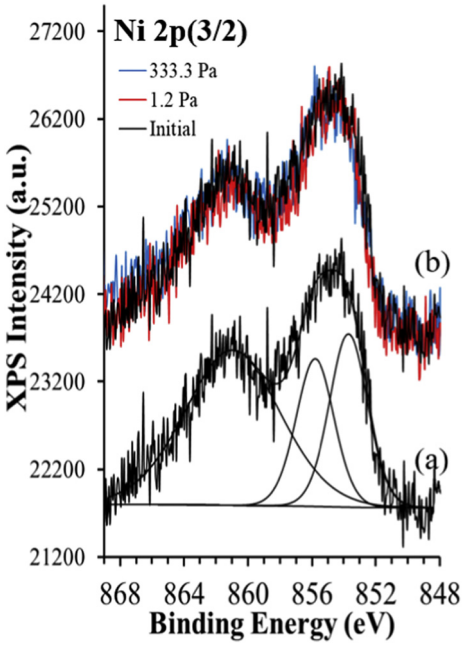

Fig. 3. Ni 2p(3/2) spectra of NiO (a) initial film. (b) An overlay of three spectra, the initial film (black) and after 1.2 Pa (red) and 333.3 Pa (blue) water vapor exposures at room temperature. (For interpretation of the references to colour in this figure legend, the reader is referred to the web version of this article.)

at 1.3×10^{-4} Pa in order to maintain a Ni^{2+} oxidation state. Fig. 3a shows an XPS spectrum in the Ni 2p(3/2) region for a freshly prepared film. The spectrum is composed of three different components consistent with the formation of NiO [20, 49] where the lowest binding energy (BE) peak observed at 853.8 eV is attributed to Ni^{2+}. The two additional peaks at 856.1 eV and 861.0 eV are consistent with NiO formation, but the origin of these peaks have been attributed to a number of effects that are still debated, including non-local screening effects, defect driven states, multi-electron charge transfer excitation processes and unscreened final state effects [49–53]. The O 1s spectrum of the freshly prepared film (Fig. 4a) shows a main feature at a BE of 529.6 eV due to the oxide (Ox) O^{2-} peak of NiO, and a smaller peak at a BE of 531.1 eV attributed to hydroxyl (OH) groups. A similar observation was observed previously for NiO/Ag(100) films, with the OH peak attributed to interaction of background water vapor with reactive edge sites [54]. The potential contribution of OH species from oxidized adventitious carbon was found to be negligible on the initial NiO film based on C 1 s results showing primarily of C—H species at 284.8 eV (Fig. 5, black spectrum). We therefore attribute the formation of OH species on the freshly prepared film to dissociation of background residual water in the vacuum chamber with highly reactive non-stoichiometric defects including edge and corner sites on the NiO islands. (See Figs. 4 and 5.)

In the subsequent experimental step, the NiO film was exposed to two separate water vapor pressures with XPS taken after each exposure. The first water vapor exposure was for 15 min. at a pressure of 1.2 Pa, corresponding to 0.04% relative humidity (RH) at 25 °C. The RH was chosen to be below the critical onset humidity of 0.01% RH, which has been shown for previous XPS studies on other metal oxide surfaces that above 0.01% RH the surface experiences significant hydroxylation events [55–58]. As seen from Fig. 4b, upon exposure to 0.04% RH there is an increase in the OH peak and evidence of a small third peak that shows up at 3.6 eV higher BE from the Ox peak which is attributed to molecularly bound water. The next water exposure was intentionally dosed above the critical onset humidity at 333.3 Pa corresponding to 10% RH for 15 min and led to a significant increase in the OH peak, a decrease in the Ox peak, while the molecularly bound water peak

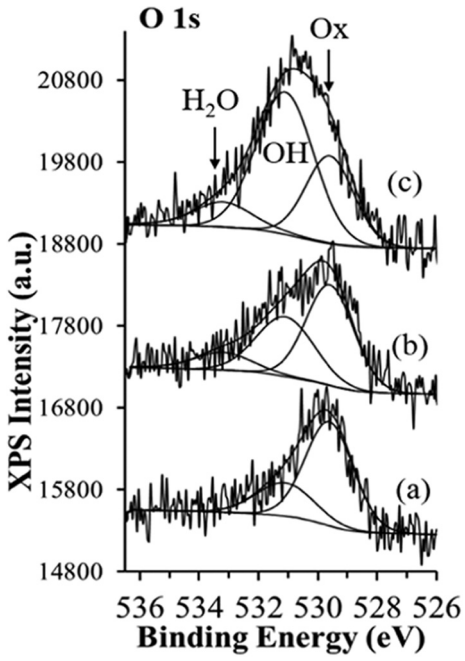

Fig. 4. O 1 s spectra of NiO (a) initial film, (b) after exposure to 1.2 Pa and (c) 333.3 Pa of water vapor. Each exposure was performed at room temperature for 15 min.

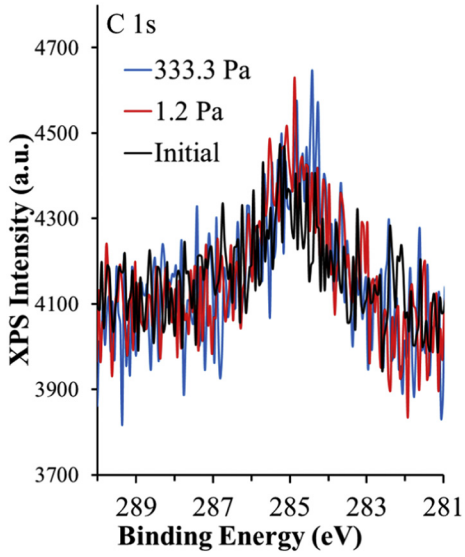

Fig. 5. C 1 s spectra of initial NiO film (black) and after water vapor exposures to 1.2 Pa (red) and 333.3 Pa (blue) at room temperature for 15 min.

remains essentially constant.

Fig. 6 shows a quantitative assessment of the O 1 s peak areas, taking the ratio of each of the three peaks to the total O 1s spectrum. Error bars are calculated from the individual errors associated with each peak fit generated from Casa XPS and propagated through the ratio calculation. The relative intensity of the OH peak goes from 0.28 up to 0.63 in going from the initial film to the 10% RH exposed film. At the same time the relative Ox peak decreases from 0.72 to 0.27. This decrease in Ox intensity is due to the conversion of the oxide sites to hydroxyl sites at the interface. The significant increase in hydroxylation in going from 0.04% to 10% RH is consistent with previous XPS observations on other metal oxides [55–58]. Moreover, a 63% OH peak area cannot be accounted for by dissociation solely at the edges of the NiO(1 × 1) islands in Fig. 1a suggesting that the observed extensive

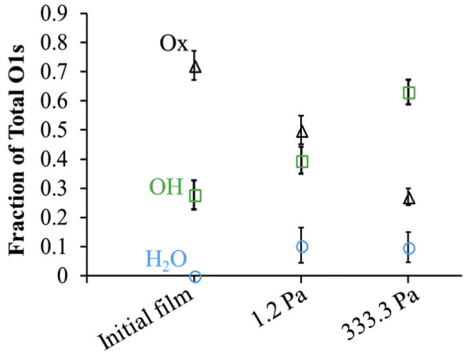

Fig. 6. Ratio of the oxide (Ox), hydroxyl (OH) and molecularly bound water (H_2O) peak to the total O 1s peak area as a function of water vapor pressure exposures preformed at room temperature were 15 min.

hydroxylation is occurring at terraces. XPS intensities of the OH and Ox species suggests that the film is 28% hydroxylated after the 0.04% RH exposure and 53% hydroxylated after the 10% RH exposure, assuming $Ni(OH)_2$ was formed.

The Ni 2p(3/2) spectral envelope remained largely unchanged upon exposure to water as seen from the overlaid spectra in Fig. 3b, suggesting that the oxidation state of Ni remains Ni^{2+} upon NiO hydroxylation. The absence of significant changes in the metal peak upon hydroxylation is not surprising and is dependent on the metal oxide being examined. For example, Fe 2p spectra are not very sensitive to hydroxylation of Fe_2O_3 in the presence of water vapor [59], whereas Mg 2p in MgO shows some evidence of peak broadening upon hydroxylation [55]. Moreover, the water vapor exposures did not lead to any change in the carbon spectra (Fig. 5). Thus, the observed increase in hydroxylation can be attributed to water adsorption.

Yang et al. [13] grew a 4 ML NiO/Ag(100) with a background water vapor pressure of $\sim 1.3 \times 10^{-7}$ Pa at 110 K and also observed three peaks in the O 1s region due to Ox, OH and molecularly bound water in the form of ice at this temperature. However, NiO/Ag(100) grown at room temperature in the same background water vapor pressure only showed two peaks (Ox and OH) similar to our spectra in Fig. 3a, and no molecularly bound water. This suggests that the higher pressures used in our study lead to extensive hydroxylation and residual adsorbed water. This is likely due to strong H_2O-OH hydrogen bonding interactions that still reside under vacuum. The existence of molecularly bound water under vacuum at room temperature is not surprising. For example, Altieri et al. [60] observed molecularly bound water on hydroxylated MgO/Ag(100) monolayer films under vacuum conditions after exposures to water vapor.

Overall our experimental results indicate that NiO monolayer films extensively hydroxylate upon exposure to near ambient water vapor pressures, while lower pressures only react at edge sites [13]. We attribute this increase in reactivity to water dissociation at terrace sites on top of the Ag(100) supported NiO film. While the XPS studies herein cannot distinguish between OH species at terrace sites versus defect sites, a peak area of 63% for OH relative to the total O 1 s peak can only be accounted for by reactions occurring at both defect sites and terraces. In the following we will further examine this hypothesis by investigating the efficacy for terrace sites to hydroxylate in the presence of adsorbed water using DFT calculations.

Let us first consider the adsorption of an isolated water molecule (1/8 ML coverage) in the non-dissociative (ND) form. Water is bound to Ni of the NiO monolayer through the O atom ($d_{Ow\text{-}Ni}$ = 2.108 Å, PBE0/A-basis) and forms with the surface a weak hydrogen bond, which leads to unequal intramolecular OH bonds (Fig. 7a). The OH group that interacts with the surface has an internuclear distance $d_{Ow\text{-}H1}$ = 0.984 Å with a short contact with the adjacent surface oxygen ($d_{Os\text{-}H1}$ = 1.860 Å, PBE0/A-basis), while the other OH distance, $d_{Ow\text{-}}$

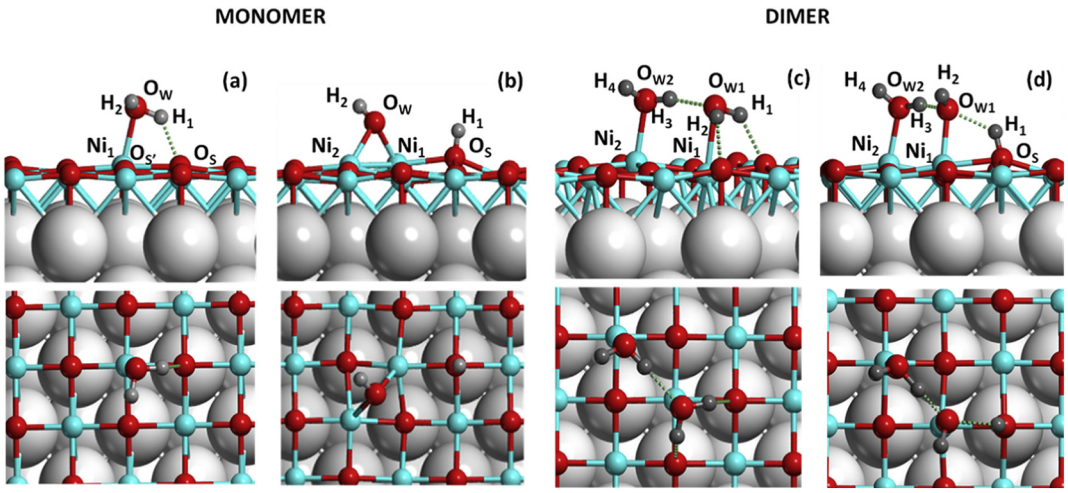

Fig. 7. Side view (top panels) and top view (bottom panels) of the geometric structure derived from DFT calculations of monolayer NiO(1 × 1)/Ag(100) with (a) non-dissociated water monomer, (b) dissociated water monomer, (c) non-dissociated water dimer and (d) dissociated water dimer. Cyan, red, dark and light grey circles correspond to Ni, O, H and Ag atoms, respectively. (For interpretation of the references to colour in this figure legend, the reader is referred to the web version of this article.)

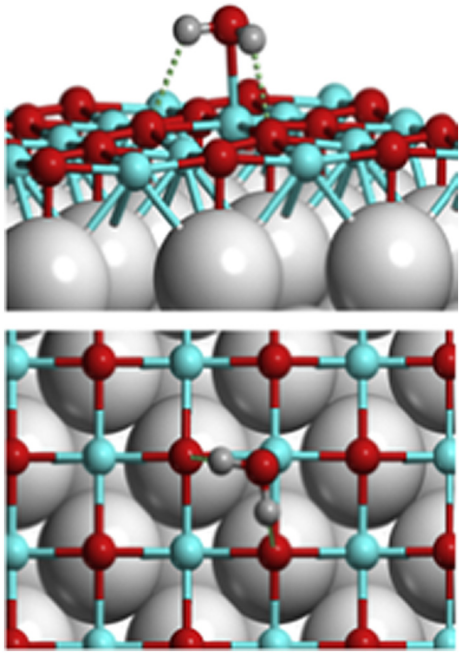

Fig. 8. Side view (top panels) and top view (bottom panels) of the geometric structure derived from DFT calculations of monolayer NiO(1 × 1)/Ag(100) with non-dissociated water in a symmetric configuration. Cyan, red, dark and light grey circles correspond to Ni, O, H and Ag atoms, respectively. (For interpretation of the references to colour in this figure legend, the reader is referred to the web version of this article.)

$_{H2}$ = 0.963 Å, is very close to the corresponding value for isolated waters (0.959 Å). The adsorption energy of this non-dissociated state is −0.68 eV/H_2O at the PBE0/A-basis level and does not change significantly when changing the basis set and DFT functional (see Table 1).

The hydrogen bond with the surface affects only marginally the stability of the adsorbate. Indeed, one could localize a different stationary point in the potential energy surface (Fig. 8) in which the water intramolecular OH bonds are almost equivalent ($d_{Ow\text{-}H1}$~ $d_{Ow\text{-}H2}$ ~0.97 Å) and similarly, distances with the adjacent surface oxygen atoms are also almost equivalent ($d_{Os\text{-}H1}$~ $d_{Os\text{-}H2}$ ~2.1 Å). In this case $E_{ads}{}^{W}$ differs by < 0.01 eV with respect to the tilted configuration demonstrating that tilting of water yields a weak hydrogen bond interaction with the substrate. Water adsorption slightly increases corrugation of the NiO monolayer. The average rumpling passes from 0.16 (bare NiO) to 0.32 Å (W-ND/NiO) with an outwards shift of 0.27 Å of the Ni cation directly bound to water. The dissociated form (D) is obtained by heterolytic splitting of the molecule with the proton bound to a surface O, $d_{Os\text{-}H1}$ = 0.963 Å, and the hydroxyl group from water was symmetrically bonded to two adjacent Ni ions, $d_{Ow\text{-}Ni1}$ = 2.012, $d_{Ow\text{-}Ni2}$ = 2.021 Å, and $d_{Ow\text{-}H2}$ = 1.085 Å (see Table 1 and Fig. 7b). Water dissociation causes a strong corrugation of the oxide layer, which is not hindered by the interaction with the metal support. The protonated surface oxygen (O_s) strongly relaxes outwards by 0.16 Å with respect to its position prior to water adsorption. The same happens to the Ni ions in contact with the adsorbed OH group, which was also lifted on average by 0.50 Å. The resulting NiO rumpling is now 0.81 Å. Such a large structural relaxation, already observed for water dissociation on MgO/Ag(100) [35] and MnO/Ag(100) films [36], is the electrostatic response to the charged nature of the dissociation fragments and contributes to the stabilization of the heterolytic dissociated state.

The adsorption of the charged fragment does not change the electronic and magnetic states of NiO: the largest variation of charge and magnetic moment (Δq = 0.05, Δμ = 0.06 e) are very small and indicate that Ni ions retain their oxidation state. Nonetheless, water dissociation leads to a significant polarization at the interface. Considering the variation of Mulliken charge in the Ag atoms at the interface we recognize a charge accumulation (Δq = 0.15|e|) in the Ag beneath the oxygen bearing the proton and a charge depletion (Δq = −0.17|e|) in the Ag atoms first neighbors to the Ni bound to the hydroxyl group. All the other Ag atoms remain unpolarized and their charge is unmodified with respect to bare Ag. Thus, at variance with the molecular adsorption, dissociated water is largely affected by the size confinement of the oxide and by the presence of the metal substrate. On the NiO monolayer supported on metals, the oxide polaronic distortion induces a strong corrugation of the film and the polarization of the metal stabilize the dissociated state. The response of the substrate makes the attraction between adsorbates with opposite charge weaker thus stabilizing the ion pair. Such a mechanism gives rise to the difference between the surface reactivity of metal supported ultrathin films and bulk oxide surfaces. The result is that unlike the NiO(100) bulk surface where the dissociated form is unstable ($E_{ads}{}^{W}$(D) = 0.43 eV/H_2O, PBE0/A results), dissociated water at the NiO(1 × 1)/Ag surface is stable ($E_{ads}{}^{W}$(D) = −0.32 eV/H_2O). However, the dissociated form is less stable than the molecular form ($E_{ads}{}^{W}$(ND) = −0.68 eV/H_2O).

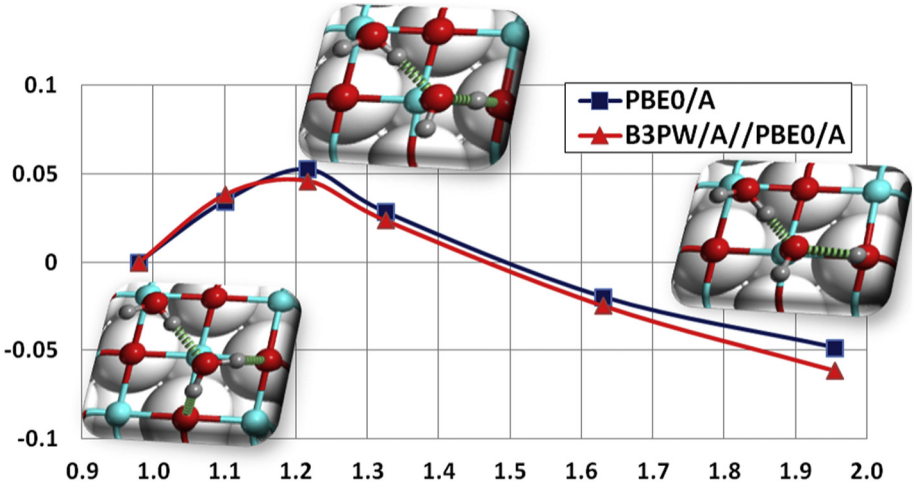

Fig. 9. DFT calculation of dissociation profile of water dimer starting from the non-dissociated dimer and leading the dissociated form. The insert depicts the structure closer to the maximum of energy in the path. See also Fig. 5 for labeling at atoms. Initial and final points of the path correspond to the structures of Fig. 5c and 5d, respectively.

Table 1
Computed properties of molecular (ND) and dissociated (D) water monomer and dimer on the NiO(1 × 1)/Ag(100) supported monolayer.

	NiO(100)1 ML/Ag(100)				
	Monomer			Dimer	
	W-ND	W-ND1	W-D	W2-ND	W2-D
$d(O_{w1}\text{-}H_1)$	0.980	0.973	3.361	0.982	1.749
$d(O_{w1}\text{-}H_2)$	0.965	0.970	0.959	0.982	0.960
$d(O_S\text{-}H_1)$	1.918	2.072	0.965	1.913	1.004
$d(O_S\text{-}H_2)$	2.476	2.080	–	1.925	–
$d(O_{w1}\text{-}Ni_1)$	2.107	2.110	2.012	2.256	1.970
$d(O_{w1}\text{-}Ni_2)$	–	–	2.021	–	–
$d(O_{w1}\text{-}O_{w2})$	–	–	–	2.834	2.613
$d(O_{w2}\text{-}H_3)$	–	–	–	0.978	1.010
$d(O_{w2}\text{-}H_4)$	–	–	–	0.960	0.960
$d(O_{w1}\text{-}H_3)$	–	–	–	1.870	1.630
$d(O_{w2}\text{-}Ni_2)$	–	–	–	2.080	2.076
$\alpha(O_{w1}\text{-}H_1\text{-}O_S)$	129.6		–	134.2	–
$\alpha(O_{w2}\text{-}H_3\text{-}O_{w1})$			–	168.3	163.3
NiO rumpling	0.32	0.32	0.81	0.32	0.63
$\Delta E_{ads}{}^{W a}$ (PBE0/A)	−0.68	−0.68	−0.32	−0.76	−0.81
$\Delta E_{ads}{}^{W a}$ (B3PW/A//PBE0/A)	−0.58	−0.58	−0.30	−0.66	−0.72
$\Delta E_{ads}{}^{W a}$ (PBE0/B//PBE0/A)	−0.64	−0.64	−0.43	−0.70	−0.78

The water coverage is 1/8 ML in all cases. Structural data refer to geometry optimizations performed at PBE0/A-basis level. Distances in Å, energies in eV. See Fig. 4 for labelling of atoms. Energies are not corrected for BSSE. However, BSSE has been estimated be < 0.15 eV with basis A and with basis B it does not exceed 0.05 eV.

[a] $\Delta E_{ads}{}^{W}$ computed with respect to free water molecules.

Starting from the molecularly adsorbed monomer, a second water molecule was added such that it also adsorbs in the proximity of a Ni atom. The interaction with the pre-adsorbed one leads to a surface aggregate (W2-ND) with an energy gain of −0.85 eV, corresponding to an on-surface dimerization which is exothermic (the energy release when two isolated monomers meet on the surface) by −0.16 eV. The adsorption energy, $E_{ads}{}^{W}$(W2-ND) = −0.76 eV/H_2O, is larger than $E_{ads}{}^{W}$ of the most stable monomer (Table 1). In the non-dissociated dimer, one molecule is symmetrically bound to the surface (Fig. 7c) with intramolecular OH bonds that have the same lengths ($d_{Ow1\text{-}H1} = d_{Ow1\text{-}H2}$ = 0.982 Å) and each one interacts with the first neighbor surface oxygen leading to similar bond distances ($d_{Os\text{-}H1} = d_{Os\text{-}H2}$ ~1.92 Å). The second water molecule is bound via a weak hydrogen bond to the adjacent one as indicated by the relatively short intermolecular distance ($d_{Ow1\text{-}H3}$ = 1.870 Å) and the intramolecular OH distance ($d_{Ow2\text{-}H3}$ = 0.978 Å) only slightly elongated with respect to a free water (Table 1).

By crossing a small energy barrier of about 0.05 eV/H_2O, where the dimer reasserts its geometry to maximize the hydrogen bond interaction with the surface (at the barrier, $d_{Ow1\text{-}H1}$ ~1.2 Å and $d_{Os\text{-}H1}$ ~1.25 Å, Fig. 9) the dimer dissociates heterolytically: the OH bond (O_{w1}-H_1) of the water molecule hydrogen bonded to the NiO breaks down leaving charged fragments (one hydroxyl group and one proton) on the surface (Fig. 5d). The hydroxyl group sits on top of a Ni atom ($d_{Ow1\text{-}Ni1}$ = 2.012 Å) and is bound via a strong hydrogen bond to the adjacent water molecule as monitored by the short intermolecular distance ($d_{Ow1\text{-}H3}$ = 1.630 Å), the intramolecular distance ($d_{Ow2\text{-}H3}$ = 1.003 Å) considerably elongated with respect to a free water and the intermolecular angle ($\alpha(O_{w2}\text{-}H_3\text{-}O_{w1})$ = 163.3°) not too far from planarity (Table 1). The proton is bound to the surface oxygen nearest neighbor to the Ni bearing the hydroxyl (Fig. 7d). The structural relaxation of NiO resembles the monomer case where the protonated surface oxygen O_s and Ni atoms in contact with the oxygen atoms of the water dimer relaxes outwards, by 0.43 and 0.42 Å, respectively (the resulting NiO rumpling is about 0.6 Å). At the same time there is a charge accumulation of −0.11 $|e|$ on the Ag atom in contact with O_sH and a charge depletion of 0.18 $|e|$ on Ag around the negatively charged fragment, which change the nature of the interaction between the charged pair compared to the bulk oxide surface. The adsorption energy of the dissociated form of the dimer ($E_{ads}{}^{W}$(W2-D) = −0.81 eV/H_2O) is slightly larger than the molecular form $E_{ads}{}^{W}$(W2-ND) by a small amount (~0.05 eV/H_2O at the PBE0/A results) but that does not change significantly when changing basis set and DFT functional (Table 1).

Despite the similarity between the dissociation of water monomer and dimer at the Ag supported monolayer, the driving force leading to stable charged products at the surface is different in the two cases. In the monomer, the polaronic distortion of the NiO film and the polarization of the conductive substrate provide the indispensable requirement to obtain stable dissociated water; in the dimer the strong intermolecular hydrogen bond in the water aggregate (between the undissociated water molecule and the hydroxyl group) plays unambiguously a relevant role to stabilize the dissociated form of the dimer.

Thus, the DFT results presented herein show that the water monomer has a stable dissociated form on Ag-supported NiO monolayer, although it is less energetically favorable compared to the molecular form. Moreover, the presence of an energy barrier to dissociation would favor the molecular form over the dissociated one. For example, a water monomer on an Ag-supported MgO monolayer has an energy barrier been estimated to exceed 0.5 eV [61]. A less energetically stable dissociate state for a water monomer is consistent with our XPS results and previous XPS experiments [13] which show minor hydroxylation when exposed to background water vapor pressures at room temperature. This also explains why former XPS, TPD and

LEED studies under low pressure water vapor exposures report that dissociation occurs only at defects and not at terraces [7–13]. Upon exposure to higher RH's, water aggregation occurs at terrace sites. The DFT results herein show that when two monomers meet on the surface they form a hydrogen bound aggregate that easily dissociates leading to a more stable product. These results are fully consistent with observations of increased hydroxylation at higher RH exposures.

4. Conclusions

Herein we examined the interaction of water vapor with NiO (1 × 1)/Ag(100) islands using vacuum-based XPS. Previous studies examining the interaction of water with NiO(100) suggested that dissociation does not occur at terrace sites when exposed to water vapor pressures in the high vacuum regime. Upon exposure to high water vapor pressures (maximum 333.3 Pa) at room temperature, we show that extensive hydroxylation is observed on Ag(100) supported NiO (1 × 1) islands. We attribute this to the dissociation of water at stoichiometric terrace sites upon aggregation. To support this interpretation we performed, DFT calculations examining the interaction of a water monomer and dimers with an Ag(100) supported NiO(1 × 1) film. Results indicate that the molecular form of a water monomer is more stable than that dissociated form. However, upon aggregation of two molecularly bound water molecules the hydrogen bounded water dimer can easily dissociate by crossing a small energy barrier, leading to a dissociated state that is more stable than the molecular dimer. This stability is mainly attributed to the H_2O-OH hydrogen bond formation and to a minor extent the structural distortion of the Ag(100) supported NiO(1 × 1) film. These results are consistent with the observations of extensive hydroxylation at higher RH exposures where aggregation is expected to occur.

Acknowledgements

This research used resources in Interface Science and Catalysis and Theory and Computation located in the Center for Functional Nanomaterials, which is a U.S. DOE Office of Science Facility at Brookhaven National Laboratory under Contract No. DE-SC0012704. J.T.N acknowledges support from a University of Delaware Research Foundation grant.

References

[1] Y. Zhang, Thermal oxidation fabrication of NiO film for optoelectronic devices, Appl. Surf. Sci. 344 (2015) 33–37.
[2] S. de Souza, S. Visco, L. De Jonghe, Thin-film solid oxide fuel cell with high performance at low-temperature, Solid State Ion 98 (1997) 57–61.
[3] D.T. Dekadjevi, A. Suvorova, S. Pogossian, D. Spenato, J. Ben Youssef, Experimental evidence for the role of nonuniform modes in the asymmetric magnetization reversal of a Ni/NiO system, Phys. Rev. B 74 (2006) 100402.
[4] I. Hotovy, J. Huran, L. Spiess, R. Capkovic, S. Hascik, Preparation and characterization of NiO thin films for gas sensor applications, Vacuum 58 (2000) 300–307.
[5] M.A. Henderson, The interaction of water with solid surfaces: fundamental aspects revisited, Surf. Sci. Rep. 46 (2002) 1–308.
[6] E. Carrasco, M.A. Brown, M. Sterrer, H. Freund, K. Kwapien, M. Sierka, J. Sauer, Thickness-dependent hydroxylation of MgO(001) thin films, J. Phys. Chem. C 114 (2010) 18207–18214.
[7] J.M. McKay, V.E. Henrich, Surface electronic structure of NiO: defect states, O_2 and H_2O interactions, Phys. Rev. B 32 (1985) 6764–6772.
[8] D. Cappus, C. Xu, D. Ehrlich, B. Dillmann, C.A. Ventrice, K. Alshamery, H. Kuhlenbeck, H.J. Freund, Hydroxyl groups on oxide surfaces: NiO(100), NiO (111) and Cr_2O_3(111), Chem. Phys. 177 (1993) 533–546.
[9] R. Reissner, U. Radke, M. Schulze, E. Umbach, Water coadsorbed with oxygen and potassium on thin NiO(100) films, Surf. Sci. 402 (1998) 71–75.
[10] M. Schulze, R. Reissner, M. Lorenz, U. Radke, W. Schnurnberger, Photoelectron study of electrochemically oxidized nickel and water adsorption on defined NiO surface layers, Electrochim. Acta 44 (1999) 3969–3976.
[11] R. Reissner, M. Schulze, Multilayer adsorption of water on NiO(100) at 120 and 143K, Surf. Sci. 454 (2000) 183–190.
[12] M. Schulze, R. Reissner, Adsorption of water on epitactic NiO(100), Surf. Sci. 482 (2001) 285–293.
[13] S. Yang, J.S. Kim, Effects of residual water molecules on growth of NiO films on ag (100), J. Korean Chem. Phys. Soc. 52 (2008) 532–535.
[14] D.J. Simpson, T. Bredow, A.R. Gerson, MSINDO study of water adsorption on NiO surfaces, Theor. Chem. Accounts 114 (2005) 242–252.
[15] D.J. Simpson, T. Bredow, A.R. Gerson, MSINDO study of acid promoted dissolution of planar MgO and NiO surfaces, J. Comput. Chem. 30 (2009) 581–588.
[16] N. Yu, W. Zhang, N. Wang, Y. Wang, B. Tang, Water adsorption on a NiO(100) surface: a GGA + U study, J. Phys. Chem. C 112 (2008) 452–457.
[17] C.J. O'Brien, Z. Rak, D.W. Brenner, Free energies of (Co, Fe, Ni, Zn)Fe_2O_4 spinels and oxides in water at high temperatures and pressure from density functional theory: results for stoichiometric NiO and $NiFe_2O_4$ surfaces, J. Phys. Condens. Matter. 25 (2013) 445008.
[18] K. Sebbari, J. Roques, C. Domain, E. Simoni, Uranyl ion interaction at the water/NiO(100) interface: a predictive investigation by first-principles molecular dynamic simulations, J. Chem. Phys. 137 (2012) 164701.
[19] C.A. Schneider, W.S. Rasband, K.W. Eliceiri, NIH image to ImageJ: 25 years of image analysis, Nat. Methods 9 (2012) 671–675.
[20] J.F. Moulder, W.F. Stickle, P.E. Sobol, K.D. Bomben, Handbook of X-Ray Photoelectron Spectroscopy, Physical Electronics, Inc., Eden Prairie, MN, 1995.
[21] G. Barcaro, I.O. Thomas, A. Fortunelli, Validation of density-functional versus density-functional plus U approaches for oxide ultrathin films, J. Chem. Phys. 132 (2010) 124703.
[22] C. Giovanardi, A. di Bona, S. Valeri, Oxygen-dosage effect on the structure and composition of ultrathin NiO layers reactively grown on ag(001), Phys. Rev. B 69 (2004) 075418.
[23] T. Bertrams, H. Neddermeyer, Growth of NiO(100) layers on Ag(100): characterization by scanning tunneling microscopy, J. Vac. Sci. Technol. B. 14 (1996) 1141–1144.
[24] I. Sebastian, T. Bertrams, K. Meinel, H. Neddermeyer, Scanning tunnelling microscopy on the growth and structure of NiO(100) and CoO(100) thin films, Faraday Discuss. 114 (1999) 129–140.
[25] C. Giovanardi, A. di Bona, S. Altieri, P. Luches, M. Liberati, F. Rossi, S. Valeri, Structure and morphology of ultrathin NiO layers on Ag(001), Thin Solid Films 428 (2003) 195–200.
[26] M. Caffio, A. Atrei, B. Cortigiani, G. Rovida, STM study of the nanostructures prepared by deposition of NiO on Ag(001), J. Phys. 18 (2006) 2379–2384.
[27] S. Grober, C. Hagendorf, H. Neddermeyer, W. Widdra, The growth of thin NiO films on Ag(001) studied by scanning tunneling microscopy and spectroscopy, Surf. Interface Anal. 40 (2008) 1741–1746.
[28] W. Steurer, F. Allegretti, S. Surnev, G. Barcaro, L. Sementa, F. Negreiros, A. Fortunelli, F.P. Netzer, Metamorphosis of ultrathin Ni oxide nanostructures on ag (100), Phys. Rev. B 84 (2011) 115446.
[29] W. Steurer, S. Surnev, A. Fortunelli, F.P. Netzer, Scanning tunneling microscopy imaging of NiO(100)(1 x 1) islands embedded in Ag(100), Surf. Sci. 606 (2012) 803–807.
[30] R. Dovesi, V.R. Saunders, C. Roetti, R. Orlando, C.M. Zicovich-Wilson, F. Pascale, B. Civalleri, K. Doll, N.M. Harrison, I.J. Bush, P. D'Arco, CRYSTAL09 User's Manual, University of Torino, Torino, 2009.
[31] A.M. Ferrari, C. Pisani, Reactivity of the non stoichiometric Ni_3O_4 phase supported at the Pd(100) surface: interaction with Au and other transition metal atoms, Phys. Chem. Chem. Phys. 10 (2008) 1463–1470.
[32] A.M. Ferrari, C. Roetti, C. Pisani, Water dissociation at MgO sub-monolayers on silver: a periodic model study, Phys. Chem. Chem. Phys. 9 (2007) 2350–2354.
[33] A.M. Ferrari, C. Pisani, An Ab initio periodic study of NiO supported at the Pd(100) surface. Part 1: the perfect epitaxial monolayer, J. Phys. Chem. B. 110 (2006) 7909–7917.
[34] A.M. Ferrari, M. Ferrero, C. Pisani, An ab initio periodic study of NiO supported at the Pd(100) surface. Part 2: the nonstoichiometric Ni_3O_4 phase, J. Phys. Chem. B. 110 (2006) 7918–7927.
[35] L. Giordano, A.M. Ferrari, Modified ion pair interaction for water dimers on supported MgO ultrathin films, J. Phys. Chem. C 116 (2012) 20349–20355.
[36] C. Arble, X. Tong, L. Giordano, A.M. Ferrari, J.T. Newberg, Water dissociation on MnO(1x1)/Ag(100), Phys. Chem. Chem. Phys. 18 (2016) 25355–25363.
[37] A. Schäfer, H. Horn, R. Ahlrichs, Fully optimized contracted Gaussian basis sets for atoms Li to Kr, J. Chem. Phys. 97 (1992) 2571–2577.
[38] P.J. Hay, W.R. Wadt, Ab initio effective core potentials for molecular calculations. Potentials for the transition metal atoms Sc to Hg, J. Chem. Phys. 82 (1985) 270–283.
[39] A.J. Thakkar, T. Koga, M. Saito, R.E. Hoffmeyer, Double and quadruple zeta contracted gaussian basis sets for hydrogen through neon, Int. J. Quantum Chem. 48 (1993) 343–354.
[40] M.F. Peintinger, D.V. Oliveira, T. Bredow, Consistent Gaussian basis sets of triple-zeta valence with polarization quality for solid-state calculations, J. Comput. Chem. 34 (2013) 451–459.
[41] S.F. Boys, F. Bernardi, Calculation of small molecular interactions by differences of separate total energies - some procedures with reduced errors, Mol. Phys. 19 (1970) 553–566.
[42] C. Adamo, V. Barone, Toward reliable density functional methods without adjustable parameters: the PBE0 model, J. Chem. Phys. 110 (1999) 6158–6170.
[43] L. Mino, A.M. Ferrari, V. Lacivita, G. Spoto, S. Bordiga, A. Zecchina, CO adsorption on anatase nanocrystals: a combined experimental and periodic DFT study, J. Phys. Chem. C 115 (2011) 7694–7700.
[44] L. Mino, G. Spoto, A.M. Ferrari, CO_2 capture by TiO_2 anatase surfaces: a combined DFT and FTIR study, J. Phys. Chem. C 118 (2014) 25016–25026.
[45] E. Balantseva, G. Berlier, B. Camino, M. Lessio, A.M. Ferrari, Surface properties of ZnS nanoparticles: a combined DFT and experimental study, J. Phys. Chem. C 118 (2014) 23853–23862.

[46] A.D. Becke, Density-functional thermochemistry. III. The role of exact exchange, J. Chem. Phys. 98 (1993) 5648–5652.
[47] J.P. Perdew, Electronic Structure of Solids' 91, Akademie Verlag, Berlin, 1991.
[48] A. Rota, S. Altieri, S. Valeri, Growth of oxide-metal interfaces by atomic oxygen: monolayer of NiO(001) on Ag(001), Phys. Rev. B 79 (2009) 161401.
[49] C. Bianchi, M. Cattania, P. Villa, XPS characterization of Ni and Mo oxides before and after insitu treatments, Appl. Surf. Sci. 70 (1993) 211–216.
[50] H. Nesbitt, D. Legrand, G. Bancroft, Interpretation of Ni 2p XPS spectra of Ni conductors and Ni insulators, Phys. Chem. Miner. 27 (2000) 357–366.
[51] A. Grosvenor, M. Biesinger, R. Smart, N. McIntyre, New interpretations of XPS spectra of nickel metal and oxides, Surf. Sci. 600 (2006) 1771–1779.
[52] D. Alders, F. Voogt, T. Hibma, G. Sawatzky, Nonlocal screening effects in 2p x-ray photoemission spectroscopy of NiO(100), Phys. Rev. B 54 (1996) 7716–7719.
[53] S. Altieri, L. Tjeng, A. Tanaka, G. Sawatzky, Core-level x-ray photoemission on NiO in the impurity limit, Phys. Rev. B 61 (2000) 13403–13409.
[54] S. Yang, J. Kim, Chemical defects in ultrathin NiO films on Ag(001), J. Korean Phys. Soc. 56 (2010) 659–665.
[55] J.T. Newberg, D.E. Starr, S. Yamamoto, S. Kaya, T. Kendelewicz, E.R. Mysak, S. Porsgaard, M.B. Salmeron, G.E. Brown, A. Nilsson, Formation of hydroxyl and water layers on MgO films studied with ambient pressure XPS, Surf. Sci. 605 (2011) 89–94.
[56] J.T. Newberg, D.E. Starr, S. Yamamoto, S. Kaya, T. Kendelewicz, E.R. Mysak, S. Porsgaard, M.B. Salmeron, G.E. Brown Jr., A. Nilsson, H. Bluhm, Autocatalytic surface hydroxylation of MgO(100) terrace sites observed under ambient conditions, J. Phys. Chem. C 115 (2011) 12864–12872.
[57] A. Shavorskiy, K. Müller, J.T. Newberg, D.E. Starr, H. Bluhm, Hydroxylation of ultrathin Al_2O_3/NiAl(110) films at environmental humidity, J. Phys. Chem. C 118 (2014) 29340–29349.
[58] T. Kendelewicz, S. Kaya, J.T. Newberg, H. Bluhm, N. Mulakaluri, W. Moritz, M. Scheffler, A. Nilsson, R. Pentcheva, G.E. Brown Jr., X-ray photoemission and density functional theory study of the interaction of water vapor with the Fe_3O_4(001) surface at near-ambient conditions, J. Phys. Chem. C 117 (2013) 2719–2733.
[59] S. Yamamoto, T. Kendelewicz, J.T. Newberg, G. Ketteler, D.E. Starr, E.R. Mysak, K.J. Andersson, H. Ogasawara, H. Bluhm, M. Salmeron, G.E. Brown Jr., A. Nilsson, Water adsorption on alpha-Fe_2O_3(0001) at near ambient conditions, J. Phys. Chem. C 114 (2010) 2256–2266.
[60] S. Altieri, S.F. Contri, S. Valeri, Hydrolysis at MgO(100)/Ag(100) oxide-metal interfaces studied by O 1s x-ray photoelectron and $MgKL_{23}L_{23}$ Auger spectroscopy, Phys. Rev. B 76 (2007) 205413.
[61] J. Jung, H. Shin, Y. Kim, M. Kawai, Controlling water dissociation on an ultrathin MgO film by tuning film thickness, Phys. Rev. B 82 (2010) 085413.